Wave Motion 70 (2017) 15–28

Contents lists available at ScienceDirect

Wave Motion

journal homepage: www.elsevier.com/locate/wavemoti

Perforated grating stacks in thin elastic plates

Michael H. Meylan [a,*], Michael J.A. Smith [b]

[a] School of Mathematical and Physical Sciences, The University of Newcastle, New South Wales 2308, Australia
[b] CUDOS ARC Centre of Excellence, School of Physics, University of Sydney, Sydney, New South Wales 2006, Australia

HIGHLIGHTS

- A boundary-element method for grating stacks in thin elastic plates is given.
- The numerical solution is validated against circular cavities solved by the multipole method.
- Results are presented for various cavity geometries.

ARTICLE INFO

Article history:
Received 30 April 2016
Received in revised form 28 July 2016
Accepted 28 July 2016
Available online 5 August 2016

Keywords:
Thin elastic plate
Biharmonic plate equation
Vibration
Gratings
Free-edge conditions

ABSTRACT

The reflection and transmission spectrum of an individual grating, and repeated stacks of gratings, is computed using boundary integral methods for arrays of arbitrarily shaped cavities, with free-edge boundary conditions, that are periodically repeated in a thin elastic plate. The solution is found using a specially developed boundary element method coupled with an array Green's function. The computational code is tested against the solution obtained using multipoles which applies only to circular geometries but is shown to give very good agreement. The code is also validated using energy balance equations which includes the evanescent modes. A number of cavity shapes are investigated and results are compared against circular cavities with equivalent volumes.

1. Introduction

Diffraction gratings are periodic structures that provide active control over the propagation of waves through media. They are extensively used in a wide range of scientific fields, with particular emphasis in the fields of optics, acoustics, chemistry and in the life sciences [1]. Through a careful choice of grating design, the controlled manipulation of light, sound, and vibrational waves can be achieved to build a wide of practical devices and to steer waves in specified directions. Despite the extensive attention paid to photonic and phononic structures, wave propagation in different systems, such as thin elastic plates, has received comparatively little research attention. This is widely regarded as being due to the extensive range of possibilities already open in photonics and phononics, but also because the governing equation for thin plates is the biharmonic operator, which is a fourth-order partial differential equation, in contrast to the Helmholtz equation, which is a second-order equation that governs wave dynamics in a wide range of periodic systems.

The study of wave propagation through thin elastic plates is commonly referred to as 'platonics' [2], and in this work we will consider plane wave propagation through gratings comprising a one-dimensional array of inclusions of arbitrary geometry. At the edges of these inclusions, free-edge boundary conditions are imposed, in an extension of previous work by some of the authors [3] on two-dimensional platonic crystals and platonic gratings with clamped-edge boundary conditions.

* Corresponding author.
E-mail address: mikemeylan@icloud.com (M.H. Meylan).

http://dx.doi.org/10.1016/j.wavemoti.2016.07.013
0165-2125/

Existing work on platonic structures has been primarily restricted to clamped and free-edge circular inclusions [4–6] or to zero-radius clamped inclusions (pins) [7–12], where semi-analytic solutions are available using multipole methods. That said, other geometries such as squares [13,14] and circular inclusions bisected with Euler–Bernoulli beams [15] have also been considered. The fundamental issue with free-edge boundary conditions is that they are intractable, even for circular inclusions, which has given rise to incorrect expressions for free-edge platonic crystals [5]. This error was found in the development of the present work, which lead to the corrected form for two-dimensional arrays of circular inclusions in [16], and in the Appendix to the present work we include the correct multipole solution for a grating of free-edge circular inclusions to avoid any possible ambiguity.

The solution method we present is a generalized boundary-integral approach [3,17]. In this setting, the periodicity of the system is embedded in quasi-periodic Green's functions which in their canonical form, are slowly converging. However a wide range of methods have been developed to accelerate their convergence [18] and these are employed in the present work. After imposing the free-edge boundary conditions in the boundary integral system, we evaluate the unknown boundary displacement and normal derivative as Fourier series and impose a solvability condition. This admits a matrix system for the unknown coefficients and gives the necessary boundary data to evaluate the reflection and transmission coefficients for the grating problem [19,3]. Incidentally, the fundamental difference between a grating and a crystal is that the domain for the grating problem is geometrically non-compact, and so there is no discrete spectrum, even though a crystal can be regarded as an infinite stack of gratings.

We emphasize that the numerical procedure presented here is intensive, and the results presented primarily serve to illustrate the method. The boundary integral method shown here is able to give a converged solution for the platonic grating problem, and we note that at present, commercially available finite element solvers have no direct framework for a solution. To obtain a finite element method solution to a one-dimensional grating problem, a finite domain must be considered, and imposing the appropriate radiation condition (i.e., imposing perfectly matched layers for the biharmonic operator) is expected to be a non-trivial task. We have developed a complete solution method for arbitrary geometries where this difficulty is entirely avoided as the Green's functions satisfy the necessary radiation conditions.

In addition to considering wave scattering by platonic gratings, we also consider stacks of gratings [20,21], and present a well-known recurrence relation procedure to determine the reflection and transmission matrices for multiple layers. For a selection of arbitrary geometry configurations (where the inclusion areas are approximately equivalent) we demonstrate that the principal orders of reflection are periodic with increasing rectangular spacing. For a single grating comprising arbitrarily shaped inclusions with two- and four-fold symmetry, the choice of inclusion geometry has a minimal effect on the transmission and reflection spectrum. However, for more complicated geometries such as Helmholtz resonators, the reflection spectra exhibits unique characteristics.

The outline of this paper is as follows. In Section 2 we present the problem formulation for wave incidence on an arbitrary grating for all boundary condition classes. In Section 3 we consider the solution for an arbitrary inclusion inside a grating cell. In Section 4 we decompose the boundary data into Helmholtz and modified Helmholtz components for use in Section 5 where we compute the reflection and transmission matrices for a single grating. In Section 6 we outline the recurrence relation procedure for multiple grating stacks. In Section 7 we present the energy balance equation for platonic gratings. This is followed in Section 8 by a selection of numerical results and concluding remarks in Section 9. Appendix presents the multipole solution for a grating of circular, free-edge inclusions.

2. Problem formulation

The governing equation for the out-of-plane displacement of a thin, elastic plate (Kirchhoff–Love plate) is the biharmonic equation

$$(\Delta^2 - k^4)w = (\Delta + k^2)(\Delta - k^2)w = 0, \tag{1}$$

where $k^2 = \omega\sqrt{\rho h/D}$, ω is the angular frequency, ρ is the mass density, h is the thickness, D is the flexural rigidity of the plate, and we have assumed a time dependence of $\exp(-\mathrm{i}\omega t)$. In this paper we consider plane wave incidence upon an array of cavities of identical shape (but arbitrary geometry) assuming free-edge boundary conditions are imposed on the edges of each hole. Following the procedure in Smith et al. [17,3], this system of equation can be decomposed into two natural field components, and we provide a brief outline for the purposes of completeness here.

Due to the linearity of the biharmonic equation the total displacement can be decomposed into incident and scattered fields, which may also be decomposed into their respective Helmholtz and modified Helmholtz components as

$$w = w_{\mathrm{I}}^{\mathrm{H}} + w_{\mathrm{S}}^{\mathrm{H}} + w_{\mathrm{I}}^{\mathrm{M}} + w_{\mathrm{S}}^{\mathrm{M}}. \tag{2}$$

Using Green's second identity with this decomposition, a boundary integral system describing a single grating is obtained [3,17] and takes the form

$$\tfrac{1}{2}w^{\mathrm{M}}(\mathbf{x}) = w_{\mathrm{I}}^{\mathrm{M}}(\mathbf{x}) + \sum_{m=-\infty}^{\infty} \int_{\partial\Omega_m} \left\{ \partial_{n'} G^{\mathrm{M}}(\mathbf{x}, \mathbf{x}') w^{\mathrm{M}}(\mathbf{x}') - \partial_{n'} w^{\mathrm{M}}(\mathbf{x}') G^{\mathrm{M}}(\mathbf{x}, \mathbf{x}') \right\} \mathrm{d}S', \tag{3a}$$

$$\tfrac{1}{2}w^{\mathrm{H}}(\mathbf{x}) = w_{\mathrm{I}}^{\mathrm{H}}(\mathbf{x}) + \sum_{m=-\infty}^{\infty}\int_{\partial\Omega_m}\left\{\partial_{n'}G^{\mathrm{H}}(\mathbf{x},\mathbf{x}')w^{\mathrm{H}}(\mathbf{x}') - \partial_{n'}w^{\mathrm{H}}(\mathbf{x}')G^{\mathrm{H}}(\mathbf{x},\mathbf{x}')\right\}\mathrm{d}S', \tag{3b}$$

for all $\mathbf{x}\in\partial\Omega_m$ where $m\in\mathbb{Z}$ and $\partial\Omega_m$ denotes the boundary of the mth inclusion. The incident fields take the form

$$w_{\mathrm{I}}^{\mathrm{H}} = \frac{\delta_0}{\sqrt{|\chi_0|}}\mathrm{e}^{\mathrm{i}\alpha_0 x - \mathrm{i}\chi_0 y}, \tag{4a}$$

$$w_{\mathrm{I}}^{\mathrm{M}} = \frac{\widehat{\delta_0}}{\sqrt{|\widehat{\chi_0}|}}\mathrm{e}^{\mathrm{i}\alpha_0 x - \mathrm{i}\hat{\chi}_0 y}, \tag{4b}$$

and $G^{\mathrm{H}}(\mathbf{x},\mathbf{x}') = \frac{\mathrm{i}}{4}H_0^{(1)}(kr)$ and $G^{\mathrm{M}}(\mathbf{x},\mathbf{x}') = \frac{\mathrm{i}}{4}H_0^{(1)}(\mathrm{i}kr)$ denote the free-space Green's functions for the Helmholtz and modified Helmholtz equations respectively, which are expressed in terms of zero-order Hankel functions, with $r = |\mathbf{x}-\mathbf{x}'|$ denoting the distance between the field and source points respectively. The normal derivatives are defined as $\partial_{n'} = (\partial_{x'}, \partial_{y'})\cdot\mathbf{n}'$ where $\mathbf{n}'$ is the outwards-pointing unit normal to the boundary, δ_0 denotes the amplitude of a Helmholtz incident wave, $\widehat{\delta_0}$ denotes the amplitude of a modified Helmholtz incident wave, $\alpha_0 = k\sin\theta_{\mathrm{i}}$, $\chi_0 = k\cos\theta_{\mathrm{i}}$, θ_{i} is the incident angle, and $\alpha_0^2 + \hat{\chi}_0^2 = -k^2$ (i.e. $\hat{\chi}_0 = \mathrm{i}\tau_0$ where $\tau_0 > 0$). We remark that the incident potentials have been scaled to simplify the conservation of energy relation presented below.

The variation in the boundary displacement field between neighbouring inclusions is given by the quasi-periodicity condition

$$w(\mathbf{x}' + (md, 0)) = w(\mathbf{x}'_m) = \mathrm{e}^{\mathrm{i}\alpha_0 md}w(\mathbf{x}'), \tag{5}$$

for the source coordinate, where d denotes the period of the grating. If we also restrict the field coordinate to the boundary of the central inclusion, then (3a)–(3b) takes the form

$$\tfrac{1}{2}w^{\mathrm{M}}(\mathbf{x}) = w_{\mathrm{I}}^{\mathrm{M}}(\mathbf{x}) + \int_{\partial\Omega_0}\left\{\partial_{n'}G_g^{\mathrm{M}}(\mathbf{x},\mathbf{x}')\,w^{\mathrm{M}}(\mathbf{x}') - \partial_{n'}w^{\mathrm{M}}(\mathbf{x}')\,G_g^{\mathrm{M}}(\mathbf{x},\mathbf{x}')\right\}\mathrm{d}S', \tag{6a}$$

$$\tfrac{1}{2}w^{\mathrm{H}}(\mathbf{x}) = w_{\mathrm{I}}^{\mathrm{H}}(\mathbf{x}) + \int_{\partial\Omega_0}\left\{\partial_{n'}G_g^{\mathrm{H}}(\mathbf{x},\mathbf{x}')\,w^{\mathrm{H}}(\mathbf{x}') - \partial_{n'}w^{\mathrm{H}}(\mathbf{x}')\,G_g^{\mathrm{H}}(\mathbf{x},\mathbf{x}')\right\}\mathrm{d}S', \tag{6b}$$

for $\mathbf{x}\in\partial\Omega_0$, where we have the quasi-periodic Green's functions

$$G_g^{\mathrm{H}}(\mathbf{x},\mathbf{x}') = \sum_{m=-\infty}^{\infty}G^{\mathrm{H}}(\mathbf{x},\mathbf{x}'_m)\mathrm{e}^{\mathrm{i}\alpha_0 md}, \tag{7a}$$

$$\partial_{n'}G_g^{\mathrm{H}}(\mathbf{x},\mathbf{x}') = \sum_{m=-\infty}^{\infty}\partial_{n'}G^{\mathrm{H}}(\mathbf{x},\mathbf{x}'_m)\mathrm{e}^{\mathrm{i}\alpha_0 md}, \tag{7b}$$

$$G_g^{\mathrm{M}}(\mathbf{x},\mathbf{x}') = \sum_{m=-\infty}^{\infty}G^{\mathrm{M}}(\mathbf{x},\mathbf{x}'_m)\mathrm{e}^{\mathrm{i}\alpha_0 md}, \tag{7c}$$

$$\partial_{n'}G_g^{\mathrm{M}}(\mathbf{x},\mathbf{x}') = \sum_{m=-\infty}^{\infty}\partial_{n'}G^{\mathrm{M}}(\mathbf{x},\mathbf{x}'_m)\mathrm{e}^{\mathrm{i}\alpha_0 md}. \tag{7d}$$

The method to compute these Green functions efficiently are given in [18,22,3]. Care must be taken with the quasi-periodic Green's function for the Helmholtz equation as it fails to converge at particular combinations of k and α_0 which correspond to Wood anomalies [23,24]. Wood anomalies occur when a diffraction order switches from being evanescent to propagating, i.e. when $\chi_m = 0$ for an $m\in\mathbb{Z}$ where

$$\chi_n = \begin{cases}\sqrt{k^2-\alpha_n^2}, & \alpha_n^2 \le k^2\\ \mathrm{i}\sqrt{\alpha_n^2-k^2}, & \alpha_n^2 > k^2,\end{cases}\qquad \widehat{\chi}_n = \mathrm{i}\sqrt{k^2+\alpha_n^2}. \tag{8}$$

However, if one adds and subtracts (6a)–(6b) together and applies the Helmholtz and modified Helmholtz operators respectively, we obtain a boundary integral system in the form

$$\tfrac{1}{2}(\Delta+k^2)w = 2k^2w_{\mathrm{I}}^{\mathrm{M}} + \int_{\partial\Omega}\left\{\partial_{n'}G_g^{\mathrm{M}}(\Delta+k^2)w - \partial_{n'}(\Delta+k^2)wG_g^{\mathrm{M}}\right\}\mathrm{d}S', \tag{9a}$$

$$\tfrac{1}{2}(\Delta-k^2)w = -2k^2w_{\mathrm{I}}^{\mathrm{H}} + \int_{\partial\Omega}\left\{\partial_{n'}G_g^{\mathrm{H}}(\Delta-k^2)w - \partial_{n'}(\Delta-k^2)wG_g^{\mathrm{H}}\right\}\mathrm{d}S', \tag{9b}$$

which is the representation considered most useful for the application of the free-edge boundary conditions.

3. Free-edge boundary conditions

The free-edge boundary conditions for a smooth cavity Stern [25] take the form

$$\Delta w = \beta \left(\partial_s^2 + \partial_s \Theta \, \partial_n\right) w, \tag{10a}$$

$$\partial_n \Delta w = \beta \left(\partial_s^2 \Theta \, \partial_s + \partial_s \Theta \, \partial_s^2 - \partial_s^2 \partial_n\right) w, \tag{10b}$$

where $\partial_s = \nabla \cdot \mathbf{s}$, $\partial_n = \nabla \cdot \mathbf{n}$, $\mathbf{s}$ is unit tangential to $\partial\Omega$, $\mathbf{n}$ and $\mathbf{n}'$ denote unit normal vectors to $\partial\Omega$ (with respect to the field and source points respectively), and $\beta = 1-\nu$, where ν is the Poisson ratio of the plate. We introduce the notation $\Theta = \Theta(s)$ for the direction cosine such that $\mathbf{n} = (\cos\Theta, \sin\Theta)$. We also assume that the cavity boundary $\partial\Omega$ is parametrized by s such that $s \in (-\gamma, \gamma)$, using the notation s and s' when referring to the field and source points respectively.

In a manner identical to Bennetts and Williams [26], we expand the resulting two unknowns (the displacement and the normal derivative of the displacement) in Eqs. (9a) and (9b) in terms of the following Fourier series

$$w(\mathbf{x}') = \sum_{m=-\infty}^{\infty} c_m \mathrm{e}^{\mathrm{i}m\pi s'/\gamma}, \qquad \partial_{n'} w(\mathbf{x}') = \sum_{m=-\infty}^{\infty} d_m \mathrm{e}^{\mathrm{i}m\pi s'/\gamma} \tag{11}$$

and then apply (10) to obtain

$$\begin{aligned}
&\sum_{m=-\infty}^{\infty} \left\{ \frac{1}{2}\left[k^2 - \beta\,(m\pi/\gamma)^2\right] \mathrm{e}^{\mathrm{i}m\pi s'/\gamma} \right\} c_m + \left\{ \frac{1}{2}\beta \partial_{s'}\Theta(s') \mathrm{e}^{\mathrm{i}m\pi s'/\gamma} \right\} d_m \\
&= 2k^2 w_{\mathrm{I}}^{\mathrm{M}} + \sum_{m=-\infty}^{\infty} c_m \left\{ \left[k^2 - \beta\,(m\pi/\gamma)^2\right] \int_{\partial\Omega} \partial_{n'} G_g^{\mathrm{M}} \mathrm{e}^{\mathrm{i}m\pi s'/\gamma} \mathrm{d}S' \right. \\
&\quad + \beta\,(m\pi/\gamma)^2 \int_{\partial\Omega} \partial_{s'}\Theta(s') G_g^{\mathrm{M}} \mathrm{e}^{\mathrm{i}m\pi s'/\gamma} \mathrm{d}S' \\
&\quad \left. - \ \mathrm{i}m\beta\pi/\gamma \int_{\partial\Omega} \partial_{s'}^2\Theta(s') G_g^{\mathrm{M}} \mathrm{e}^{\mathrm{i}m\pi s'/\gamma} \mathrm{d}S' \right\} \\
&\quad + d_m \left\{ \beta \int_{\partial\Omega} \partial_{s'}\Theta(s') \partial_{n'} G_g^{\mathrm{M}} \mathrm{e}^{\mathrm{i}m\pi s'/\gamma} \mathrm{d}S' \right. \\
&\quad \left. - \left[k^2 + \beta\,(m\pi/\gamma)^2\right] \int_{\partial\Omega} G_g^{\mathrm{M}} \mathrm{e}^{\mathrm{i}m\pi s'/\gamma} \mathrm{d}S' \right\},
\end{aligned} \tag{12a}$$

and

$$\begin{aligned}
&\sum_{m=-\infty}^{\infty} \left\{ \frac{1}{2}\beta \partial_{s'}\Theta(s') \mathrm{e}^{\mathrm{i}m\pi s'/\gamma} \right\} d_m - \left\{ \frac{1}{2}\left[k^2 + \beta\,(m\pi/\gamma)^2\right] \mathrm{e}^{\mathrm{i}m\pi s'/\gamma} \right\} c_m \\
&= -2k^2 w_{\mathrm{I}}^{\mathrm{H}} + \sum_{m=-\infty}^{\infty} c_m \left\{ -\left[k^2 + \beta\,(m\pi/\gamma)^2\right] \int_{\partial\Omega} \partial_{n'} G_g^{\mathrm{H}} \mathrm{e}^{\mathrm{i}m\pi s'/\gamma} \mathrm{d}S' \right. \\
&\quad + \beta\,(m\pi/\gamma)^2 \int_{\partial\Omega} \partial_{s'}\Theta(s') G_g^{\mathrm{H}} \mathrm{e}^{\mathrm{i}m\pi s'/\gamma} \mathrm{d}S' \\
&\quad \left. - \mathrm{i}m\beta\pi/\gamma \int_{\partial\Omega} \partial_{s'}^2\Theta(s') G_g^{\mathrm{H}} \mathrm{e}^{\mathrm{i}m\pi s'/\gamma} \mathrm{d}S' \right\} \\
&\quad + d_m \left\{ \beta \int_{\partial\Omega} \partial_{s'}\Theta(s') \partial_{n'} G_g^{\mathrm{H}} \mathrm{e}^{\mathrm{i}m\pi s'/\gamma} \mathrm{d}S' \right. \\
&\quad \left. + \left[k^2 - \beta\,(m\pi/\gamma)^2\right] \int_{\partial\Omega} G_g^{\mathrm{H}} \mathrm{e}^{\mathrm{i}m\pi s'/\gamma} \mathrm{d}S' \right\}.
\end{aligned} \tag{12b}$$

Multiplying these resulting expressions by $\mathrm{e}^{\mathrm{i}n\pi s/\gamma}$, truncating the Fourier series, and integrating over the cavity boundary $\partial\Omega_0$ with respect to the field point yields the block-matrix system:

$$\mathbf{M}\mathbf{z} = \left[\begin{array}{c|c} \mathbf{M}_{11} & \mathbf{M}_{12} \\ \hline \mathbf{M}_{21} & \mathbf{M}_{22} \end{array}\right] \mathbf{z} = \mathbf{f}, \tag{13}$$

with the component blocks of $\mathbf{M}$ defined as

$$\mathbf{M}_{11} = \left[\frac{1}{2}\left(k^2\mathbf{I} - \eta\mathbf{N}^2\right)\mathbf{G} + \xi\mathbf{N}\mathbf{B}^{\mathrm{M}} - \eta\mathbf{N}^2\mathbf{A}^{\mathrm{M}} - \left(k^2\mathbf{I} - \eta\mathbf{N}^2\right)\mathbf{E}^{\mathrm{M}} \right], \tag{14a}$$

$$\mathbf{M}_{12} = \left[\frac{1}{2}\beta\mathbf{H} - \beta\mathbf{C}^{\mathrm{M}} + \left(k^2\mathbf{I} + \eta\mathbf{N}^2\right)\mathbf{D}^{\mathrm{M}}\right] \tag{14b}$$

$$\mathbf{M}_{21} = \left[\left(k^2\mathbf{I} + \eta\mathbf{N}^2\right)\mathbf{E}^{\mathrm{H}} + \xi\mathbf{N}\mathbf{B}^{\mathrm{H}} - \eta\mathbf{N}^2\mathbf{A}^{\mathrm{H}} - \frac{1}{2}\left(k^2\mathbf{I} + \eta\mathbf{N}^2\right)\mathbf{G}\right] \tag{14c}$$

$$\mathbf{M}_{22} = \left[\frac{1}{2}\beta\mathbf{H} - \beta\mathbf{C}^{\mathrm{H}} - \left(k^2\mathbf{I} - \eta\mathbf{N}^2\right)\mathbf{D}^{\mathrm{H}}\right], \tag{14d}$$

where $\mathbf{I}$ denotes the identity matrix, $\mathbf{z} = [c_N, \ldots, c_{-N}, d_N, \ldots, d_{-N}]^{\mathrm{T}}$, $\mathbf{f} = [\mathbf{g}^{\mathrm{M}}, \mathbf{g}^{\mathrm{H}}]^{\mathrm{T}}$, $\xi = i\beta\pi/\gamma$, $\eta = \beta\pi^2/\gamma^2$,

$$\mathbf{A}^{\mathrm{M,H}}_{mn} = \int_{\partial\Omega}\int_{\partial\Omega} \partial_{s'}\Theta(s')G^{\mathrm{M,H}}\mathrm{e}^{\mathrm{i}m\pi s'/\gamma}\mathrm{e}^{\mathrm{i}n\pi s/\gamma}\mathrm{d}S'\mathrm{d}S, \qquad \mathbf{G}_{mn} = \int_{\partial\Omega}\mathrm{e}^{\mathrm{i}(m+n)\pi s/\gamma}\mathrm{d}S,$$

$$\mathbf{B}^{\mathrm{M,H}}_{mn} = \int_{\partial\Omega}\int_{\partial\Omega} \partial^2_{s'}\Theta(s')G^{\mathrm{M,H}}\mathrm{e}^{\mathrm{i}m\pi s'/\gamma}\mathrm{e}^{\mathrm{i}n\pi s/\gamma}\mathrm{d}S'\mathrm{d}S, \qquad \mathbf{H}_{mn} = \int_{\partial\Omega}\partial_s\Theta(s)\mathrm{e}^{\mathrm{i}(m+n)\pi s/\gamma}\mathrm{d}S,$$

$$\mathbf{C}^{\mathrm{M,H}}_{mn} = \int_{\partial\Omega}\int_{\partial\Omega} \partial_{s'}\Theta(s')\partial_{n'}G^{\mathrm{M,H}}\mathrm{e}^{\mathrm{i}m\pi s'/\gamma}\mathrm{e}^{\mathrm{i}n\pi s/\gamma}\mathrm{d}S'\mathrm{d}S, \qquad \mathbf{N}_{mn} = n\delta_{mn}, \quad \text{and}$$

$$\mathbf{D}^{\mathrm{M,H}}_{mn} = \int_{\partial\Omega}\int_{\partial\Omega} G^{\mathrm{M,H}}\mathrm{e}^{\mathrm{i}m\pi s'/\gamma}\mathrm{e}^{\mathrm{i}n\pi s/\gamma}\mathrm{d}S'\mathrm{d}S, \qquad \mathbf{g}^{\mathrm{H}_n} = -2k^2\int_{\partial\Omega} w_{\mathrm{I}}^{\mathrm{H}}\mathrm{e}^{\mathrm{i}n\pi s/\gamma}\mathrm{d}S,$$

$$\mathbf{E}^{\mathrm{M,H}}_{mn} = \int_{\partial\Omega}\int_{\partial\Omega} \partial_{n'}G^{\mathrm{M,H}}\mathrm{e}^{\mathrm{i}m\pi s'/\gamma}\mathrm{e}^{\mathrm{i}n\pi s/\gamma}\mathrm{d}S'\mathrm{d}S, \qquad \mathbf{g}^{\mathrm{M}_n} = 2k^2\int_{\partial\Omega} w_{\mathrm{I}}^{\mathrm{M}}\mathrm{e}^{\mathrm{i}n\pi s/\gamma}\mathrm{d}S.$$

After having solved this system, we possess the c_m and d_m coefficients necessary to compute the displacement w and the normal derivative $\partial_n w$ at the edge of the inclusion. In order to construct the reflection and transmission matrices for this free edge plate structure, it is necessary to decompose these fields into Helmholtz and modified Helmholtz components.

4. Decomposition of the boundary data

At the boundary of the central inclusion we remark once more that the total displacement and normal derivative fields can be decomposed as

$$w\big|_{\partial\Omega} = w^{\mathrm{H}}\big|_{\partial\Omega} + w^{\mathrm{M}}\big|_{\partial\Omega} = \sum_{m=-\infty}^{\infty} c_m\mathrm{e}^{\mathrm{i}m\pi s/\gamma}, \tag{15}$$

$$\partial_n w\big|_{\partial\Omega} = \partial_n w^{\mathrm{H}}\big|_{\partial\Omega} + \partial_n w^{\mathrm{M}}\big|_{\partial\Omega} = \sum_{m=-\infty}^{\infty} d_m\mathrm{e}^{\mathrm{i}m\pi s/\gamma}, \tag{16}$$

where

$$(\Delta + k^2)w^{\mathrm{H}}\big|_{\partial\Omega} = 0, \tag{17a}$$

$$(\Delta - k^2)w^{\mathrm{M}}\big|_{\partial\Omega} = 0. \tag{17b}$$

Substituting these expansions into the boundary conditions (10) and solving the resulting system ultimately gives the relationship between the total fields and the decomposed fields as

$$w^{\mathrm{H}}\big|_{\partial\Omega} = \frac{1}{2}\sum_{m=-\infty}^{\infty}\{c_m - e_m\}\,\mathrm{e}^{\mathrm{i}m\pi s/\gamma}, \tag{18a}$$

$$w^{\mathrm{M}}\big|_{\partial\Omega} = \frac{1}{2}\sum_{m=-\infty}^{\infty}\{c_m + e_m\}\,\mathrm{e}^{\mathrm{i}m\pi s/\gamma}, \tag{18b}$$

$$\partial_n w^{\mathrm{H}}\big|_{\partial\Omega} = \frac{1}{2}\sum_{m=-\infty}^{\infty}\{d_m - f_m\}\,\mathrm{e}^{\mathrm{i}m\pi s/\gamma}, \tag{18c}$$

$$\partial_n w^{\mathrm{M}}\big|_{\partial\Omega} = \frac{1}{2}\sum_{m=-\infty}^{\infty}\{d_m + f_m\}\,\mathrm{e}^{\mathrm{i}m\pi s/\gamma}, \tag{18d}$$

where

$$e_m = \frac{\beta}{k^2}\left[\partial_s\Theta d_m - \frac{m^2\pi^2}{\gamma^2}c_m\right] \tag{19a}$$

$$f_m = \frac{\beta}{k^2}\left[\partial_s^2\Theta\left(\frac{\mathrm{i}m\pi}{\gamma}\right)c_m - \left(\frac{m^2\pi^2}{\gamma^2}\right)(\partial_s\Theta\, c_m + d_m)\right]. \tag{19b}$$

Using the decomposed fields (18a)–(18d), the total displacement of the plate exterior to the cavity can be determined by simply adding (6a) and (6b) together and multiplying by a factor of two. This method was used in [17] but here we focus on the reflection and transmission properties of thin plates, and so we now proceed to the evaluation of the reflection and transmission matrices for a single grating.

5. Reflection and transmission matrices

The derivation of the reflection and transmission coefficients of a platonic grating with a periodically repeated arbitrary inclusion can be found in Smith et al. [3]. These are presented explicitly using a double superscript notation for the boundary data, where the first superscript refers to the Helmholtz or modified Helmholtz component of the field, and the second superscript refers to the incident wave type. For example, w^{MH} denotes the w^{M} field for a Helmholtz incident wave $w_{\mathrm{I}}^{\mathrm{H}}$. The derivation of the coefficients is involved and for compactness we simply state the final expressions which take the form

$$R_m^{\mathrm{H}} = \frac{|\chi_m|}{2\mathrm{i}d\chi_m}\int_{\partial\Omega_0}\left\{v_m^{\mathrm{H}}(\mathbf{x}';-\chi_m)\partial_{n'}w^{\mathrm{HH}}(\mathbf{x}') - w^{\mathrm{HH}}(\mathbf{x}')\partial_{n'}v_m^{\mathrm{H}}(\mathbf{x}';-\chi_m)\right\}\mathrm{d}S', \tag{20a}$$

$$\widehat{R}_m^{\mathrm{M}} = -\frac{1}{2d}\int_{\partial\Omega_0}\left\{v_m^{\mathrm{M}}(\mathbf{x}';-\widehat{\chi}_m)\partial_{n'}w^{\mathrm{MM}}(\mathbf{x}') - w^{\mathrm{MM}}(\mathbf{x}')\partial_{n'}v_m^{\mathrm{M}}(\mathbf{x}';-\widehat{\chi}_m)\right\}\mathrm{d}S', \tag{20b}$$

$$R_m^{\mathrm{M}} = \frac{|\chi_m|}{2\mathrm{i}d\chi_m}\int_{\partial\Omega_0}\left\{v_m^{\mathrm{H}}(\mathbf{x}';-\chi_m)\partial_{n'}w^{\mathrm{HM}}(\mathbf{x}') - w^{\mathrm{HM}}(\mathbf{x}')\partial_{n'}v_m^{\mathrm{H}}(\mathbf{x}';-\chi_m)\right\}\mathrm{d}S'. \tag{20c}$$

$$\widehat{R}_m^{\mathrm{H}} = -\frac{1}{2d}\int_{\partial\Omega_0}\left\{v_m^{\mathrm{M}}(\mathbf{x}';-\widehat{\chi}_m)\partial_{n'}w^{\mathrm{MH}}(\mathbf{x}') - w^{\mathrm{MH}}(\mathbf{x}')\partial_{n'}v_m^{\mathrm{M}}(\mathbf{x}';-\widehat{\chi}_m)\right\}\mathrm{d}S' \tag{20d}$$

and

$$T_m^{\mathrm{H}} = \delta_{m0} + \frac{|\chi_m|}{2\mathrm{i}d\chi_m}\int_{\partial\Omega_0}\left\{v_m^{\mathrm{H}}(\mathbf{x}';\chi_m)\partial_{n'}w^{\mathrm{HH}}(\mathbf{x}') - w^{\mathrm{HH}}(\mathbf{x}')\partial_{n'}v_m^{\mathrm{H}}(\mathbf{x}';\chi_m)\right\}\mathrm{d}S', \tag{21a}$$

$$\widehat{T}_m^{\mathrm{M}} = \delta_{m0} - \frac{1}{2d}\int_{\partial\Omega_0}\left\{v_m^{\mathrm{M}}(\mathbf{x}';\widehat{\chi}_m)\partial_{n'}w^{\mathrm{MM}}(\mathbf{x}') - w^{\mathrm{MM}}(\mathbf{x}')\partial_{n'}v_m^{\mathrm{M}}(\mathbf{x}';\widehat{\chi}_m)\right\}\mathrm{d}S', \tag{21b}$$

$$T_m^{\mathrm{M}} = \frac{|\chi_m|}{2\mathrm{i}d\chi_m}\int_{\partial\Omega_0}\left\{v_m^{\mathrm{H}}(\mathbf{x}';\chi_m)\partial_{n'}w^{\mathrm{HM}}(\mathbf{x}') - w^{\mathrm{HM}}(\mathbf{x}')\partial_{n'}v_m^{\mathrm{H}}(\mathbf{x}';\chi_m)\right\}\mathrm{d}S', \tag{21c}$$

$$\widehat{T}_m^{\mathrm{H}} = -\frac{1}{2d}\int_{\partial\Omega_0}\left\{v_m^{\mathrm{M}}(\mathbf{x}';\widehat{\chi}_m)\partial_{n'}w^{\mathrm{MH}}(\mathbf{x}') - w^{\mathrm{MH}}(\mathbf{x}')\partial_{n'}v_m^{\mathrm{M}}(\mathbf{x}';\widehat{\chi}_m)\right\}\mathrm{d}S', \tag{21d}$$

where

$$v_m^{\mathrm{H}} = \frac{1}{\sqrt{|\mu_m|}}\mathrm{e}^{-\mathrm{i}\alpha_m x+\mathrm{i}\mu_m y}, \tag{22a}$$

$$v_m^{\mathrm{M}} = \frac{1}{\sqrt{|\widehat{\mu}_m|}}\mathrm{e}^{-\mathrm{i}\alpha_m x+\mathrm{i}\widehat{\mu}_m y}, \tag{22b}$$

and $\mu_m = \pm\chi_m$ or $\widehat{\mu}_m = \pm\widehat{\chi}_m$ denote plane wave incidence from above and below the grating. These expressions are used to generate the component blocks of the reflection and transmission matrices for a single grating and take the form

$$\mathbf{R}^{(0)} = \left[\begin{array}{c|c}\mathbf{R}_{\mathrm{HH}}^{(0)} & \mathbf{R}_{\mathrm{HM}}^{(0)}\\ \hline \mathbf{R}_{\mathrm{MH}}^{(0)} & \mathbf{R}_{\mathrm{MM}}^{(0)}\end{array}\right], \quad \text{and} \quad \mathbf{T}^{(0)} = \left[\begin{array}{c|c}\mathbf{T}_{\mathrm{HH}}^{(0)} & \mathbf{T}_{\mathrm{HM}}^{(0)}\\ \hline \mathbf{T}_{\mathrm{MH}}^{(0)} & \mathbf{T}_{\mathrm{MM}}^{(0)}\end{array}\right], \tag{23}$$

where the phase origin is taken to be at $y = 0$. Explicitly the component matrices are defined as

$$\left[\mathbf{R}_{\mathrm{HH}}^{(0)}\right]_{pq} = R_p^{\mathrm{H}}, \qquad \left[\mathbf{R}_{\mathrm{HM}}^{(0)}\right]_{pq} = R_p^{\mathrm{M}}, \qquad \left[\mathbf{R}_{\mathrm{MH}}^{(0)}\right]_{pq} = \widehat{R}_p^{\mathrm{H}}, \qquad \left[\mathbf{R}_{\mathrm{MM}}^{(0)}\right]_{pq} = \widehat{R}_p^{\mathrm{M}} \tag{24}$$

for an incident wave field travelling down the channel $\alpha_q = \alpha_0 + 2\pi q/d$. The transmission matrix $\mathbf{T}^{(0)}$ is populated in an analogous manner.

Having determined the reflection and transmission matrices for a single grating, we now proceed to the problem of grating stacks.

6. Scattering by a multiple gratings

We begin by introducing the matrices $\mathbf{R}_1$, $\mathbf{T}_1$, which are identical to the matrices in (23) except that the phase origins have been translated by half the grating translation vector $\tau = (0, \eta)$. These matrices are defined as

$$\mathbf{R}_1 = \mathbf{P}\mathbf{R}^{(0)}\mathbf{P}, \qquad \mathbf{T}_1 = \mathbf{P}\mathbf{T}^{(0)}\mathbf{P}, \tag{25}$$

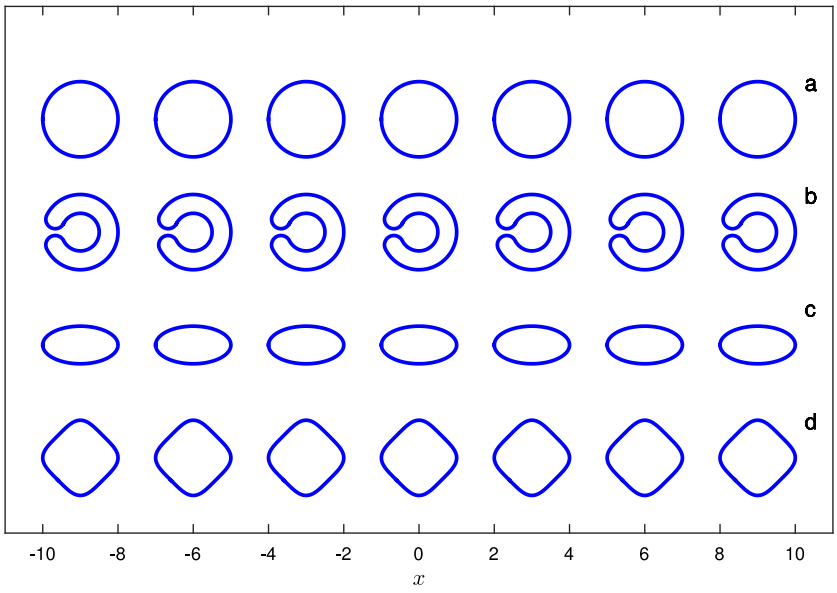

Fig. 1. A schematic diagram to scale of the four different arrays we consider first with simple inclusion geometries.

where

$$\mathbf{P} = \left[\begin{array}{c|c} \mathbf{P}^{\mathrm{H}} & \mathbf{0} \\ \hline \mathbf{0} & \mathbf{P}^{\mathrm{M}} \end{array}\right], \quad \mathbf{P}^{\mathrm{H}}_{pq} = \delta_{pq} \mathrm{e}^{\mathrm{i}\chi_p \eta/2}, \quad \mathbf{P}^{\mathrm{M}}_{pq} = \delta_{pq} \mathrm{e}^{\mathrm{i}\widehat{\chi}_p \eta/2}. \tag{26}$$

Next we use the recurrence relation expression given in [21,2] to obtain (assuming symmetry)

$$\mathbf{R}_2 = \mathbf{R}_1 + \mathbf{T}_1 \mathbf{R}_1 \left(\mathbf{I} - \mathbf{R}_1 \mathbf{R}_1\right)^{-1} \mathbf{T}_1, \tag{27a}$$

$$\mathbf{T}_2 = \mathbf{T}_1 \left(\mathbf{I} - \mathbf{R}_1 \mathbf{R}_1\right)^{-1} \mathbf{T}_1, \tag{27b}$$

which are the reflection and transmission matrices for a grating pair. The phase origin is then recentred by pre- and post-multiplying these matrices by $\mathbf{P}^{-1}$ following (25).

We can extend these relations to more than two gratings recursively as

$$\mathbf{R}_{n+1} = \mathbf{R}_1 + \mathbf{T}_1 \mathbf{R}_n \left(\mathbf{I} - \mathbf{R}_1 \mathbf{R}_n\right)^{-1} \mathbf{T}_1, \tag{28a}$$

$$\mathbf{T}_{n+1} = \mathbf{T}_n \left(\mathbf{I} - \mathbf{R}_1 \mathbf{R}_n\right)^{-1} \mathbf{T}. \tag{28b}$$

7. Energy balance equations

As a check on numerics we use the previously computed conservation of energy relation as given in [19,3]. We express it in the following matrix form:

$$\mathbf{R}_n^{\mathrm{T}} \mathbf{U} \mathbf{R}_n^* + \mathbf{T}_n^{\mathrm{T}} \mathbf{U} \mathbf{T}_n^* = \mathbf{U} - \mathrm{i}\left(\mathbf{V}\mathbf{R}_n^* - \mathbf{R}_n^{\mathrm{T}} \mathbf{V}^{\mathrm{T}}\right), \tag{29}$$

where the subscript n refers to any number of grating stacks with

$$\mathbf{U} = \left[\begin{array}{c|c} \mathbf{U}^{\mathrm{H}} & \mathbf{0} \\ \hline \mathbf{0} & \mathbf{0} \end{array}\right], \quad \mathbf{V} = \left[\begin{array}{c|c} \mathbf{V}^{\mathrm{H}} & \mathbf{0} \\ \hline \mathbf{0} & \mathbf{V}^{\mathrm{M}} \end{array}\right], \tag{30a}$$

$$\mathbf{U}^{\mathrm{H}}_{pq} = \beta_p \delta_{pq}, \qquad \mathbf{V}^{\mathrm{H}}_{pq} = (\beta_p - 1)\delta_{pq}, \qquad \mathbf{V}^{\mathrm{M}}_{pq} = \delta_{pq}, \qquad \beta_n = \begin{cases} 1, & \alpha_n^2 \leq k^2 \\ 0, & \alpha_n^2 > k^2, \end{cases} \tag{30b}$$

and star notation represents a complex conjugate operation. The relation (30a) is satisfied independent of the order of truncation. We use this energy balance equation and a further check on our numerics as it applies to the arbitrary shaped cavities.

8. Results

We begin by considering the four different cavity geometries shown in Fig. 1 (to scale).

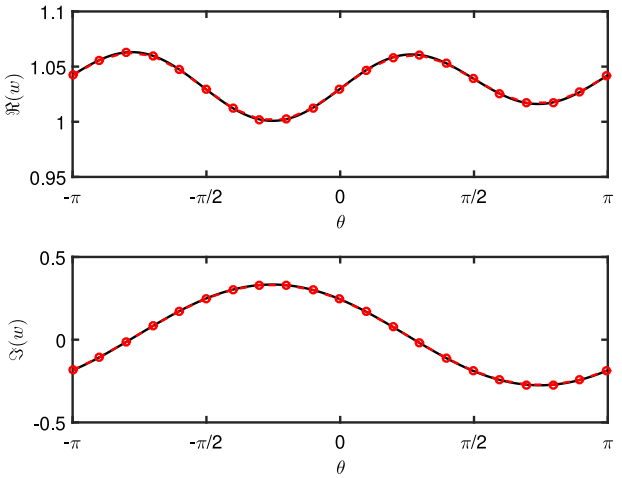

Fig. 2. The real and imaginary parts of the displacement around the edge of a circular array of cavities calculated by the multipole method (solid black line) and by the general shape code (red dashed line with circles). The incident wave direction was $\theta_i = \pi/4$, the wavenumber was $k = 1.5$, the radius was $a = 0.2$, Young's modulus was $\nu = 0.3$ and the lattice spacing was $d = 1.5$. (For interpretation of the references to colour in this figure legend, the reader is referred to the web version of this article.)

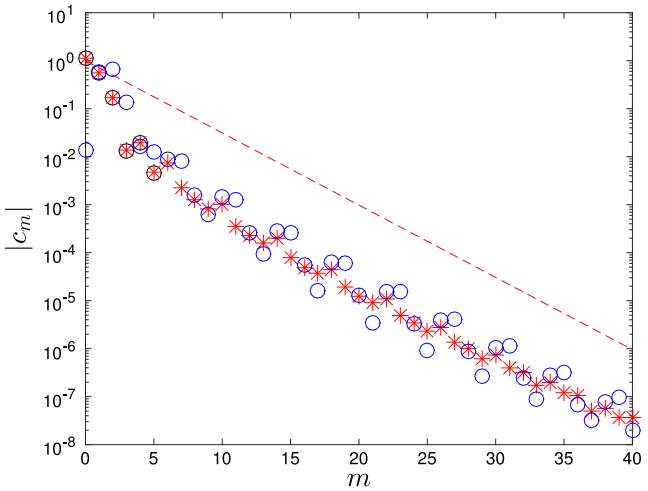

Fig. 3. The absolute value of c_m versus m for an array geometry of type (d) at normal incidence. The red stars denote $k = 1$ with $N = 40$, and the blue circles denote $N = 40$ with $k = 2$. The dashed line shows $|c_m| = \left(\sqrt{1/2}\right)^m$. (For interpretation of the references to colour in this figure legend, the reader is referred to the web version of this article.)

The dimensions of these different shapes are scaled to ensure their areas are approximately similar to a circular cavity of radius one and the spacing between the cavities is set to be $d = 3$, unless otherwise specified.

We first test the code by comparing with the calculation for circular cavities by a multipole method (see Appendix). Fig. 2 shows the real and imaginary parts of the displacement around the edge of the circle calculated by the multipole method (black solid line) and by the general method we have presented here (red dashed line with circles). Here, excellent agreement can be seen. It should be noted that through this comparison we were able to find a small error in the solution for a circular array given by Movchan et al. [5]; the correct expression was given in [16].

We now briefly consider convergence of the Fourier series expansions for the decomposed boundary data. Naturally, the solution depends on the number of panels and the number of Fourier modes N. In Fig. 3 we consider the convergence of c_m with the number of Fourier modes corresponding the diamond shape (d). We specify a suitably large number of panels, specify $k = 1$ or $k = 2$ and consider incident Helmholtz plane waves at normal incidence. Here we observe that the value of c_m gets smaller as $\left(\sqrt{1/2}\right)^m$.

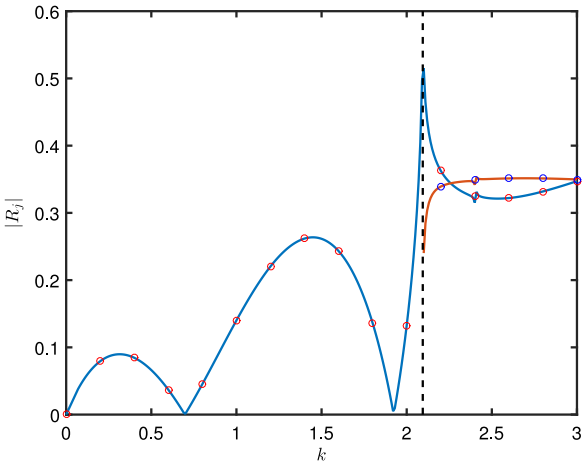

Fig. 4. The first reflection coefficient $|R_0|$(blue line) and the second reflection coefficient $|R_1|$(red line) for a circular array as in Fig. 1(a) as a function of k. The circles are the same calculation using the multipole code. The dashed black vertical line is the first cut-off at $k = 2\pi/3$. (For interpretation of the references to colour in this figure legend, the reader is referred to the web version of this article.)

We now consider the circular array as shown in Fig. 1(a). Fig. 4 shows the reflection coefficients for this geometry at normal incidence. We plot the absolute value of the reflection coefficients $|R_j|$ for j corresponding to travelling waves only (and not evanescent waves). The first cut-off (Wood anomaly) is at $k = 2\pi/3$, which is marked by the vertical black line, so above this we have two reflection curves. The solid line is the calculation using our general code and the circles show the solution found using the multipole expansion. Excellent agreement can be seen between the two methods.

In Fig. 5 we present the same results as in Fig. 4 except for the remaining three geometries shown in Fig. 1. We also plot the solution for the circular cavities given in Fig. 4 for comparison. We observe a minimal qualitative difference in the reflection spectra for these different geometries.

Fig. 6 shows the coefficient of the first reflection coefficient for multiple arrays as a function of the array spacing. The solid black line corresponds to a stack of two arrays, the dashed blue line is for 3 arrays and the chained red line is for four arrays. Subfigure (a) is for the array of circles, subfigure (b) is for the array of clover shapes, subfigure (c) is for the array of ellipses and subfigure (d) is for the array diamond shapes. The wavenumber was $k = 1.5$ and results were computed at normal incidence. The results show again that there is little qualitative difference between the shapes. It is interesting to note the points of perfect transmission (when the reflection is zero) which such systems exhibit.

Finally, we consider more complex geometries as shown in Fig. 7 which we regard as different Helmholtz resonator designs. They are constructed using two partial circles of different radii that are joined by circles at their ends. Geometry (g) is formed by rotating geometry (e) by $\pi/4$. In Fig. 8 the absolute value of the reflection coefficient R_0 is presented at normal incidence (solid line) and at $\theta_i = \pi/4$ (dashed line). This final figure is particularly interesting in that perfect reflection is observed at discrete frequencies in the spectrum.

9. Conclusions

We have shown that the problem of an array of arbitrary shaped cavities can be solved using a special boundary element method for the most difficult case (and also the most practical case) of free-edge conditions. We have validated our method against the solution for a circular cavity calculated using a multipole expansion. We have also validated our code using an energy balance relation.

A range of numerical results have been presented which are intended primarily to validate and to showcase our bespoke numerical code. For the geometries we consider here, the difference between the results for the circle and for the non-circular geometries were shown to qualitatively similar. However, for inclusion geometries with internal cavities (such as Helmholtz resonators) results were markedly different, exhibiting strong reflection at fixed frequencies.

Appendix. Multipole solution for free-edge circular inclusions

In this appendix we outline the multipole approach to obtain the displacement (and its normal derivative) at the edge of a circular inclusion, which forms part of a one-dimensional array and begin with the multipole expansion of the biharmonic plate equation for a homogeneous problem, which takes the form

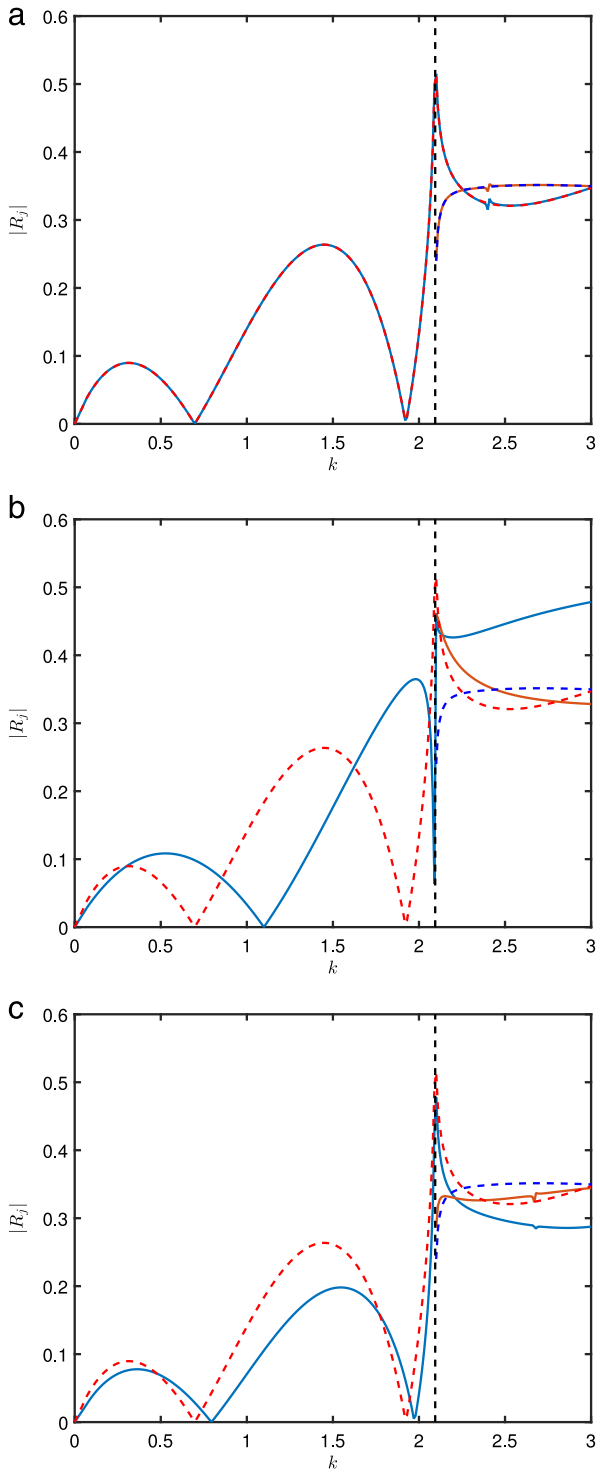

Fig. 5. The reflection coefficient as a function of k as in Fig. 4 except that we also plot the solution for the circular array as a dashed line. Subfigure (a) is the four leaf clover shape shown in Fig. 1(b). Subfigure (b) is the four leaf clover shape shown in Fig. 1(c). Subfigure (c) is the four leaf clover shape shown in Fig. 1(d).

$$w(\mathbf{x}) = \sum_{n=-\infty}^{\infty} \left[A_n J_n(kr) + E_n H_n^{(1)}(kr) + B_n I_n(kr) + F_n K_n(kr)\right] \mathrm{e}^{\mathrm{i}n\theta} \tag{A.1}$$

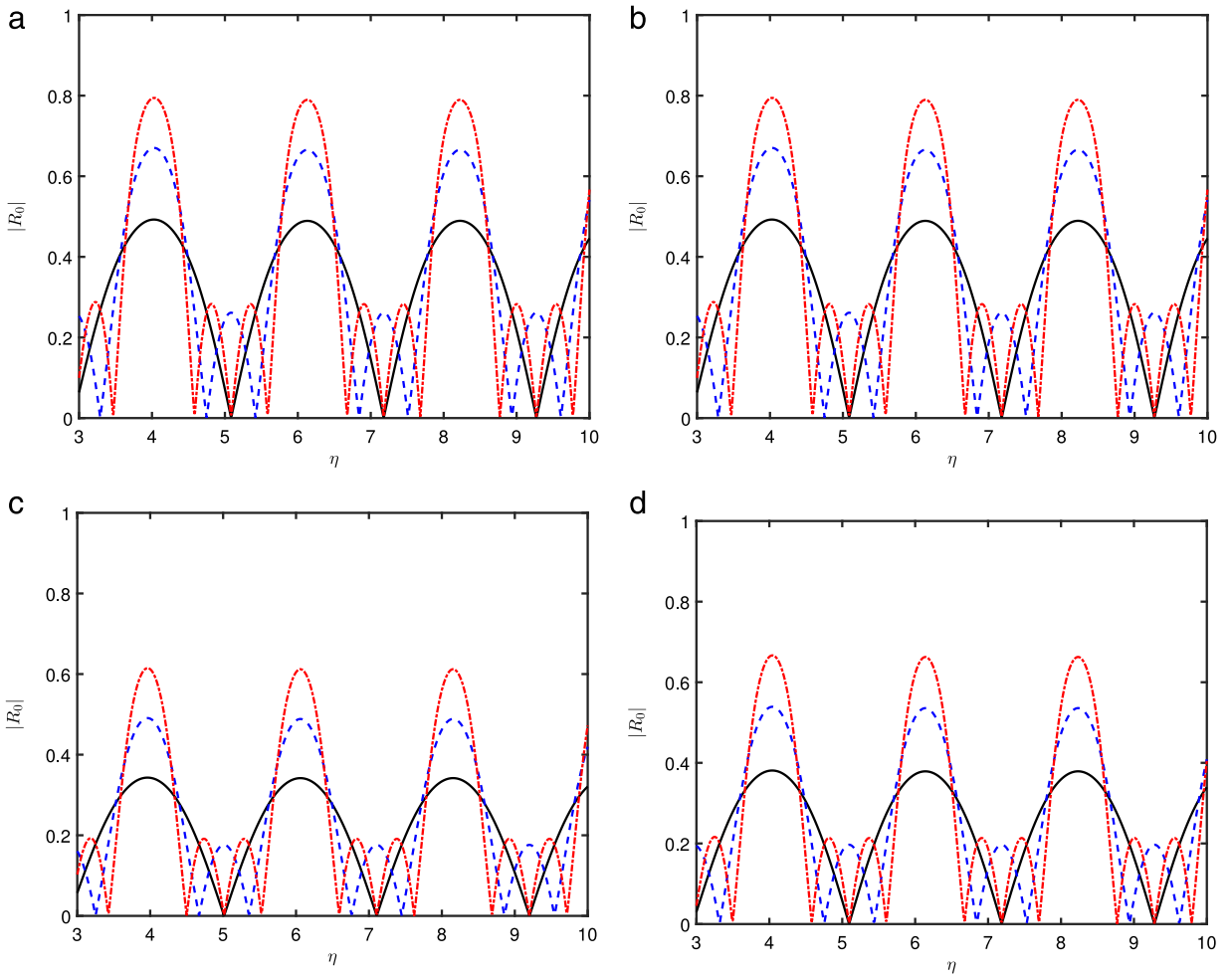

Fig. 6. The reflection coefficient $|R_0|$ for the first mode for normal incidence as a function of the array spacing η for two (black solid line) three (blue dashed line) and four (red) chained line. Subfigure (a) is for the array of four leaf clover shaped cavities, Subfigure (b) is for the array of elliptical cavities, and Subfigure (c) is for the array of diamond shaped cavities. (For interpretation of the references to colour in this figure legend, the reader is referred to the web version of this article.)

where the incident plane wave fields have the expansions [2]

$$w_{\mathrm{I}}^{\mathrm{H}}(\mathbf{x}) = \frac{\delta_0}{\sqrt{|\chi_0|}} \mathrm{e}^{\mathrm{i}\alpha_0 x - \mathrm{i}\chi_0 y} = \frac{\delta_0}{\sqrt{|\chi_0|}} \sum_{l=-\infty}^{\infty} \mathrm{i}^l \left(\frac{\alpha_0 + \mathrm{i}\chi_0}{k} \right)^l J_l(kr) \mathrm{e}^{\mathrm{i}l\theta}, \tag{A.2a}$$

$$w_{\mathrm{I}}^{\mathrm{M}}(\mathbf{x}) = \frac{\widehat{\delta}_0}{\sqrt{|\widehat{\chi}_0|}} \mathrm{e}^{\mathrm{i}\alpha_0 x - \mathrm{i}\widehat{\chi}_0 y} = \frac{\widehat{\delta}_0}{\sqrt{|\widehat{\chi}_0|}} \sum_{l=-\infty}^{\infty} \mathrm{i}^l \left(\frac{\alpha_0 + \mathrm{i}\widehat{\chi}_0}{k} \right)^l I_l(kr) \mathrm{e}^{\mathrm{i}l\theta}. \tag{A.2b}$$

The dynamic Rayleigh identities below, which encapsulate information about the incident wave potentials are

$$A_n = \sum_{m=-\infty}^{\infty} (-1)^{n+m} S_{m-n}^{\mathrm{H,G}} E_m + \frac{\delta_0}{\sqrt{|\chi_0|}} \mathrm{i}^n \left(\frac{\alpha_0 + \mathrm{i}\chi_0}{k} \right)^n, \tag{A.3a}$$

$$B_n = \sum_{m=-\infty}^{\infty} (-1)^{m} S_{m-n}^{\mathrm{K,G}} F_m + \frac{\widehat{\delta}_0}{\sqrt{|\widehat{\chi}_0|}} \mathrm{i}^n \left(\frac{\alpha_0 + \mathrm{i}\widehat{\chi}_0}{k} \right)^n, \tag{A.3b}$$

one obtains the system

$$\sum_{l=-\infty}^{\infty} \Big\{ (-1)^{l+n} S_{l-n}^{\mathrm{H,G}}(k, \boldsymbol{\kappa}) \left[-(1-\nu) ka J_n'(ka) + \left((1-\nu) n^2 - k^2 a^2 \right) J_n(ka) \right] + \delta_{ln} \left[-(1-\nu) ka H_n^{(1)\prime}(ka) + \left((1-\nu) n^2 - k^2 a^2 \right) H_n^{(1)}(ka) \right] \Big\} E_l$$

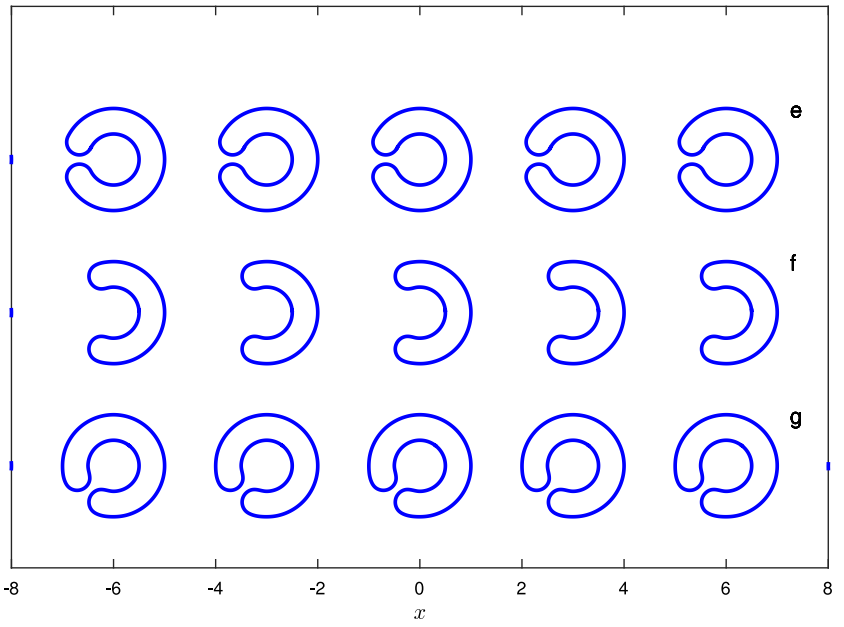

Fig. 7. A schematic diagram to scale of the three Helmholtz resonator geometries considered.

$$
\begin{aligned}
&+\sum_{l=-\infty}^{\infty}\Big\{(-1)^{l}S^{\mathrm{K,G}}_{l-n}(k,\boldsymbol{\kappa})\left[-(1-\nu)kaI_n'(ka)+\left((1-\nu)n^2+k^2a^2\right)I_n(ka)\right]\\
&+\delta_{ln}\left[-(1-\nu)kaK_n'(ka)+\left((1-\nu)n^2+k^2a^2\right)K_n(ka)\right]\Big\}F_l\\
&=-\frac{\delta_0}{\sqrt{|\chi_0|}}\mathrm{i}^n\left(\frac{\alpha_0+\mathrm{i}\chi_0}{k}\right)^n\left[-(1-\nu)kaJ_n'(ka)+\left((1-\nu)n^2-k^2a^2\right)J_n(ka)\right]\\
&-\frac{\widehat{\delta}_0}{\sqrt{|\widehat{\chi}_0|}}\mathrm{i}^n\left(\frac{\alpha_0+\mathrm{i}\widehat{\chi}_0}{k}\right)^n\left[-(1-\nu)kaI_n'(ka)+\left((1-\nu)n^2+k^2a^2\right)I_n(ka)\right],
\end{aligned}
\tag{A.4a}
$$

and

$$
\begin{aligned}
&\sum_{l=-\infty}^{\infty}\Big\{(-1)^{l+n}S^{\mathrm{H,G}}_{l-n}(k,\boldsymbol{\kappa})\left[(1-\nu)n^2J_n(ka)-\left((1-\nu)n^2ka+k^3a^3\right)J_n'(ka)\right]\\
&+\delta_{ln}\left[(1-\nu)n^2H_n^{(1)}(ka)-\left((1-\nu)n^2ka+k^3a^3\right)H_n^{(1)\prime}(ka)\right]\Big\}E_l\\
&+\sum_{l=-\infty}^{\infty}\Big\{(-1)^{l}S^{\mathrm{K,G}}_{l-n}(k,\boldsymbol{\kappa})\left[(1-\nu)n^2I_n(ka)+\left(-(1-\nu)n^2ka+k^3a^3\right)I_n'(ka)\right]\\
&+\delta_{ln}\left[(1-\nu)n^2K_n(ka)+\left(-(1-\nu)n^2ka+k^3a^3\right)K_n'(ka)\right]\Big\}F_l\\
&=-\frac{\delta_0}{\sqrt{|\chi_0|}}\mathrm{i}^n\left(\frac{\alpha_0+\mathrm{i}\chi_0}{k}\right)^n\left[(1-\nu)n^2J_n(ka)-\left((1-\nu)n^2ka+k^3a^3\right)J_n'(ka)\right]\\
&-\frac{\widehat{\delta}_0}{\sqrt{|\widehat{\chi}_0|}}\mathrm{i}^n\left(\frac{\alpha_0+\mathrm{i}\widehat{\chi}_0}{k}\right)^n\left[(1-\nu)n^2I_n(ka)+\left(-(1-\nu)n^2ka+k^3a^3\right)I_n'(ka)\right].
\end{aligned}
\tag{A.4b}
$$

If the sums in the above are truncated, this admits a block matrix system of the form

$$
\begin{bmatrix}A_{11} & A_{12}\\ A_{21} & A_{22}\end{bmatrix}\begin{bmatrix}\mathbf{E}\\ \mathbf{F}\end{bmatrix}=\begin{bmatrix}\mathbf{f}_1\\ \mathbf{f}_2\end{bmatrix}
\tag{A.5}
$$

which can be solved directly for E_n and F_n.

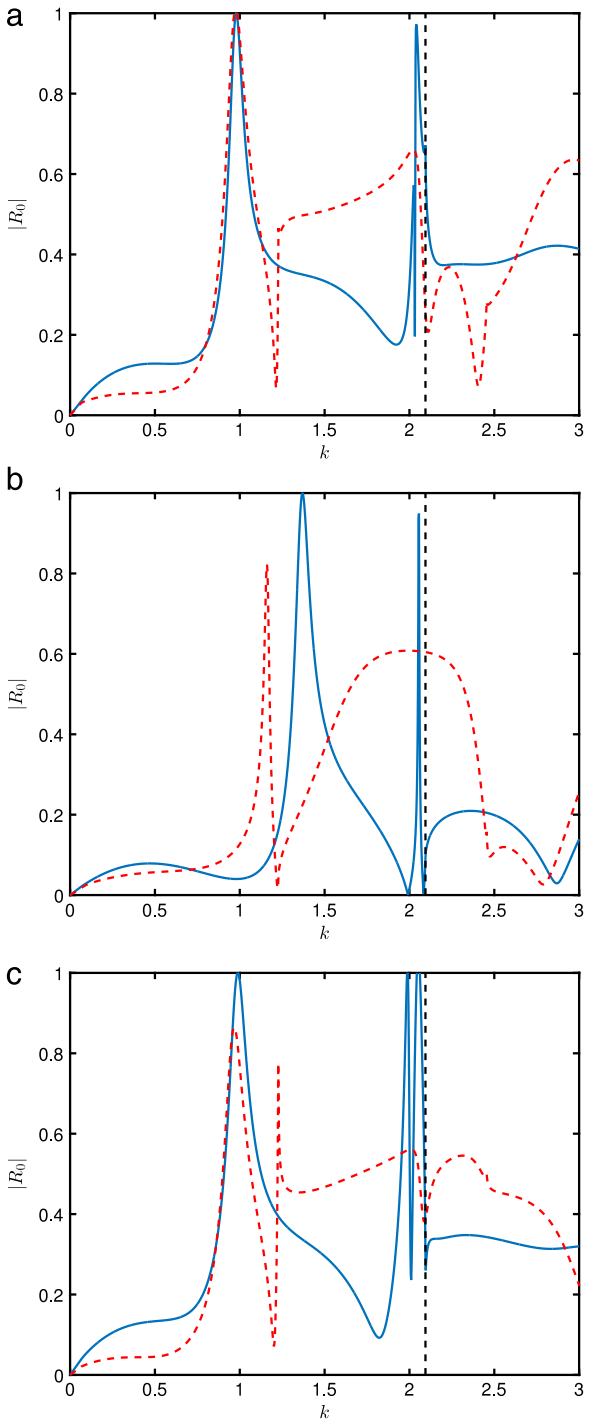

Fig. 8. Reflection coefficient $|R_0|$ as a function of k as in Fig. 4 for (a) geometry (e) in Fig. 7, (b) geometry (f) of Fig. 7, and (c) geometry (g) of Fig. 7. The solid line denotes normal incidence and the dashed line refers to $\theta_i = \pi/4$.

References

[1] E. Popov, Gratings: Theory and Numeric Applications, Popov, Institut Fresnel, 2012.
[2] R.C. McPhedran, A.B. Movchan, N.V. Movchan, Platonic crystals: Bloch bands, neutrality and defects, Mech. Mater. 41 (4) (2009) 356–363.
[3] M.J.A. Smith, M.H. Meylan, R.C. McPhedran, Flexural wave filtering and platonic polarisers in thin elastic plates, Quart. J. Mech. Appl. Math. 66 (4) (2013) 437–463.
[4] A. Norris, C. Vemula, Scattering of flexural waves on thin plates, J. Sound Vib. 181 (1) (1995) 115–125.

[5] A.B. Movchan, N.V. Movchan, R.C. McPhedran, Bloch–Floquet bending waves in perforated thin plates, Proc. R. Soc. A: Math. Phys. Eng. Sci. 463 (2086) (2007) 2505.
[6] C.G. Poulton, R.C. McPhedran, N.V. Movchan, A.B. Movchan, Convergence properties and flat bands in platonic crystal band structures using the multipole formulation, Waves Random Complex Media 20 (4) (2010) 702–716.
[7] D.V. Evans, R. Porter, Flexural waves on a pinned semi-infinite thin elastic plate, Wave Motion 45 (6) (2008) 745–757.
[8] D. Evans, R. Porter, Penetration of flexural waves through a periodically constrained thin elastic plate in vacuo and floating on water, J. Eng. Math. 58 (1) (2007) 317–337.
[9] M.J.A. Smith, R.C. McPhedran, C.G. Poulton, M.H. Meylan, Negative refraction and dispersion phenomena in platonic clusters, Waves Random Complex Media 22 (4) (2012) 435–458.
[10] M.J.A. Smith, R. Porter, T.D. Williams, The effect on bending waves by defects in pinned elastic plates, J. Sound Vib. 331 (23) (2012) 5087–5106.
[11] M.J.A. Smith, R.C. McPhedran, M.H. Meylan, Double Dirac cones at k= 0 in pinned platonic crystals, Waves Random Complex Media 24 (1) (2014) 35–54.
[12] R.C. McPhedran, A.B. Movchan, N.V. Movchan, M. Brun, M.J.A. Smith, Parabolic trapped modes and steered Dirac cones in platonic crystals, in: Proceedings of the Royal Society A: Mathematical, Physical and Engineering Science, Vol. 471, The Royal Society, 2015, p. 20140746.
[13] M. Farhat, S. Guenneau, S. Enoch, High directivity and confinement of flexural waves through ultra-refraction in thin perforated plates, Europhys. Lett. 91 (5) (2010) 54003.
[14] M. Dubois, M. Farhat, E. Bossy, S. Enoch, S. Guenneau, P. Sebbah, Flat lens for pulse focusing of elastic waves in thin plates, Appl. Phys. Lett. 103 (7) (2013) 071915.
[15] A. Climente, A.N. Norris, J. Sánchez-Dehesa, Scattering of flexural waves from a hole in a thin plate with an internal beam, J. Acoust. Soc. Am. 137 (1) (2015) 293–302.
[16] M.J.A. Smith, M.H. Meylan, R.C. McPhedran, C.G. Poulton, A short remark on the band structure of free-edge platonic crystals, Waves Random Complex Media 24 (4) (2014) 421–430.
[17] M.J.A. Smith, M.H. Meylan, R.C. McPhedran, Scattering by cavities of arbitrary shape in an infinite plate and associated vibration problems, J. Sound Vib. 330 (16) (2011) 4029–4046.
[18] C.M. Linton, The Green's function for the two-dimensional Helmholtz equation in periodic domains, J. Engrg. Math. 33 (4) (1998) 377–401.
[19] N.V. Movchan, R.C. McPhedran, A.B. Movchan, C.G. Poulton, Wave scattering by platonic grating stacks, Proc. R. Soc. A: Math. Phys. Eng. Sci. 465 (2111) (2009) 3383.
[20] L.C. Botten, N.A. Nicorovici, R.C. McPhedran, M. de Sterke, A.A. Asatryan, Photonic band structure calculations using scattering matrices, Phys. Rev. E 64 (4) (2001) 046603.
[21] S.B. Platts, N.V. Movchan, R.C. McPhedran, A.B. Movchan, Two–dimensional phononic crystals and scattering of elastic waves by an array of voids, Proc. R. Soc. Lond. Ser. A Math. Phys. Eng. Sci. 458 (2026) (2002) 2327–2347.
[22] N.A. Nicorovici, R.C. McPhedran, Lattice sums for off–axis electromagnetic scattering by gratings, Phys. Rev. E 50 (4) (1994) 3143–3160.
[23] R.W. Wood, XLII. On a remarkable case of uneven distribution of light in a diffraction grating spectrum, Lond. Edinb. Dublin Philos. Mag. J. Sci. 4 (21) (1902) 396–402.
[24] L. Rayleigh, Note on the remarkable case of diffraction spectra described by Prof. Wood, Lond. Edinb. Dublin Philos. Mag. J. Sci. 14 (79) (1907) 60–65.
[25] M. Stern, A general boundary integral formulation for the numerical solution of plate bending problems, Internat. J. Solids Struct. 15 (10) (1979) 769–782.
[26] L.G. Bennetts, T.D. Williams, Wave scattering by ice floes and polynyas of arbitrary shape, J. Fluid Mech. 662 (2010) 5–35.